THE ASTROPHYSICAL JOURNAL, 546:1027–1037, 2001 January 10
© 2001. The American Astronomical Society. All rights reserved. Printed in U.S.A.

BROADBAND SPECTRUM OF CYGNUS X-1 IN TWO SPECTRAL STATES WITH *BeppoSAX*

F. FRONTERA,[1,2] E. PALAZZI,[2] A. A. ZDZIARSKI,[3] F. HAARDT,[4] G. C. PEROLA,[5] L. CHIAPPETTI,[6] G. CUSUMANO,[7] D. DAL FIUME,[2] S. DEL SORDO,[7] M. ORLANDINI,[2] A. N. PARMAR,[8] L. PIRO,[9] A. SANTANGELO,[7] A. SEGRETO,[7] A. TREVES,[4] AND M. TRIFOGLIO[2]

Received 2000 June 6; accepted 2000 September 5

ABSTRACT

We report on the 0.5–200 keV spectral properties of Cyg X-1 observed at different epochs with the Narrow Field Instruments of the *BeppoSAX* satellite. The source was in its soft state during the first observation of 1996 June. In the second observation of 1996 September, the source had parameters characteristic to its hard state. A soft X-ray excess, a broad Fe Kα line and Compton reflection are clearly detected in both states. The soft-state broadband continuum is well modeled by a disk blackbody (accounting for the soft excess) and Compton upscattering of the disk photons by a hybrid, thermal/nonthermal plasma, probably forming a corona above the disk (also giving rise to the Compton-reflection component). In the hard state, the primary hard X-ray spectrum can be well modeled by Compton upscattering of a weak blackbody emission by a thermal plasma at a temperature of ~ 60 keV. The soft excess is then explained by thermal Comptonization of the same blackbody emission by another hot plasma cloud characterized by a low value of its Compton parameter. Finally, we find the characteristic ratio of the bolometric flux in the soft state to that in the hard state to be about 3. This value is much more compatible with theories of state transitions than the previously reported (and likely underestimated) value of 1.5.

Subject headings: accretion, accretion disks — binaries: general — black hole physics — stars: individual (Cygnus X-1) — X-rays: stars

1. INTRODUCTION

Cyg X-1 is one of the brightest and most extensively studied X-ray sources in the sky. Its optical companion is the O9.7 Iab supergiant HDE 226868. Estimates of the mass, M, of the X-ray star, $5 \lesssim M/M_{\odot} \lesssim 15$ (e.g., Herrero et al. 1995), strongly suggest the presence of a black hole.

Its distance has been claimed to be $d \gtrsim 2.5$ kpc based on comparison of the extinction of Cyg X-1, $E(B-V) \sim 1.0$–1.1, with that of field stars (Bregman et al. 1973; Margon, Bowyer, & Stone 1973). On the other hand, HDE 226868 belongs, most likely, to the NGC 6871/OB3 association (Massey, Johnson, & DeGioia-Eastwood 1995), in which case a large fraction of the extinction is local to the association. The distance to the association was measured as $d \approx 1.8 \pm 0.5$ kpc (Janes & Adler 1982), 2.1 ± 0.1 kpc (Massey et al. 1995), and 1.8 kpc (Malysheva 1997). Here, we adopt $d = 2$ kpc, which is also the value assumed by Gierliński et al. (1999, hereafter G99).

On timescales from weeks to years, the 2–10 keV flux typically shows two intensity states: a low state, in which the source spends $\sim 90\%$ of the time, characterized by a luminosity of L(2–10 keV) $\sim 3 \times 10^{36}$ ergs s^{-1} and by a hard power-law spectrum ($\propto E^{-\Gamma}$) with a photon spectral index of $\Gamma \sim 1.7$ (e.g., Gierliński et al. 1997, hereafter G97), and a high state corresponding to a 2–10 keV luminosity an order of magnitude higher, with a strong blackbody component with $kT \sim 0.5$ keV and soft power-law tail with $\Gamma \sim 2$–3 (Dolan et al. 1977; Ogawara et al. 1982). Based on these spectral properties, we will hereafter call the states hard (HS) and soft (SS). The low-energy ($\lesssim 10$ keV) and the high-energy ($\gtrsim 20$ keV) fluxes are anticorrelated in the two states (see review by Liang & Nolan 1984), while the bolometric luminosity changes weakly (Nowak 1995; Zhang et al. 1997b).

Based on the shape of the high-energy cutoff to the power-law spectrum in the HS, the dominant radiative process appears to be thermal Comptonization (Sunyaev & Trümper 1979; Nolan et al. 1981; Phlips et al. 1996; G97). The seed photons for this process are, most likely, provided by blackbody emission of some cold medium, a component of which is also seen in the HS at low energies (e.g., Ebisawa et al. 1996, hereafter E96). The cold medium probably forms an accretion disk, as indicated by the presence of Compton reflection (Done et al. 1992; G97) and a fluorescent Fe Kα emission (Done et al. 1992; E96; G97).

In 1996 May, Cyg X-1 underwent a transition (see Fig. 1) from the HS to the SS, with an increase of the 2–10 keV flux (Cui 1996) and a decrease of the 20–200 keV flux (Zhang et al. 1996). The SS lasted until 1996 September and, during that period, several X-ray observations were performed. Belloni et al. (1996) report on observations with the *Rossi X-Ray Timing Explorer*'s Proportional Counter Array (*RXTE*/PCA) on May 22, 23, and 30, and one in 1996 February, when the source was in its normal HS. The May spectra were fit with a "multicolor" blackbody model (Mitsuda et al. 1984) with $kT_{\rm in} = 0.36 \pm 0.01$ keV at the

[1] Dipartimento di Fisica, Università degli Studi di Ferrara, Via Paradiso 12, I-44100 Ferrara, Italy; frontera@fe.infn.it.
[2] Istituto Tecnologie e Studio Radiazioni Extraterrestri, CNR, Via Gobetti 101, 40129 Bologna, Italy.
[3] N. Copernicus Astronomical Center, Bartycka 18, 00-716 Warsaw, Poland; aaz@camk.edu.pl.
[4] Università dell'Insubria, Via Lucini 3, I-22100 Como, Italy.
[5] Dipartimento di Fisica "E. Amaldi," Università degli Studi "Roma Tre," Via della Vasca Navale 84, I-00146 Roma, Italy.
[6] Istituto di Fisica Cosmica "G. Occhialini," CNR, Via Bassini 15, I-20133 Milano, Italy.
[7] Istituto di Fisica Cosmica ed Applicazioni dell'Informatica, CNR, Via U. La Malfa 153, I-90146 Palermo, Italy.
[8] Astrophysics Division, Space Science Department of ESA, 2200 AG Noordwijk, Netherlands.
[9] Istituto di Astrofisica Spaziale, CNR, Via Fosso del Cavaliere, I-00133 Roma, Italy.

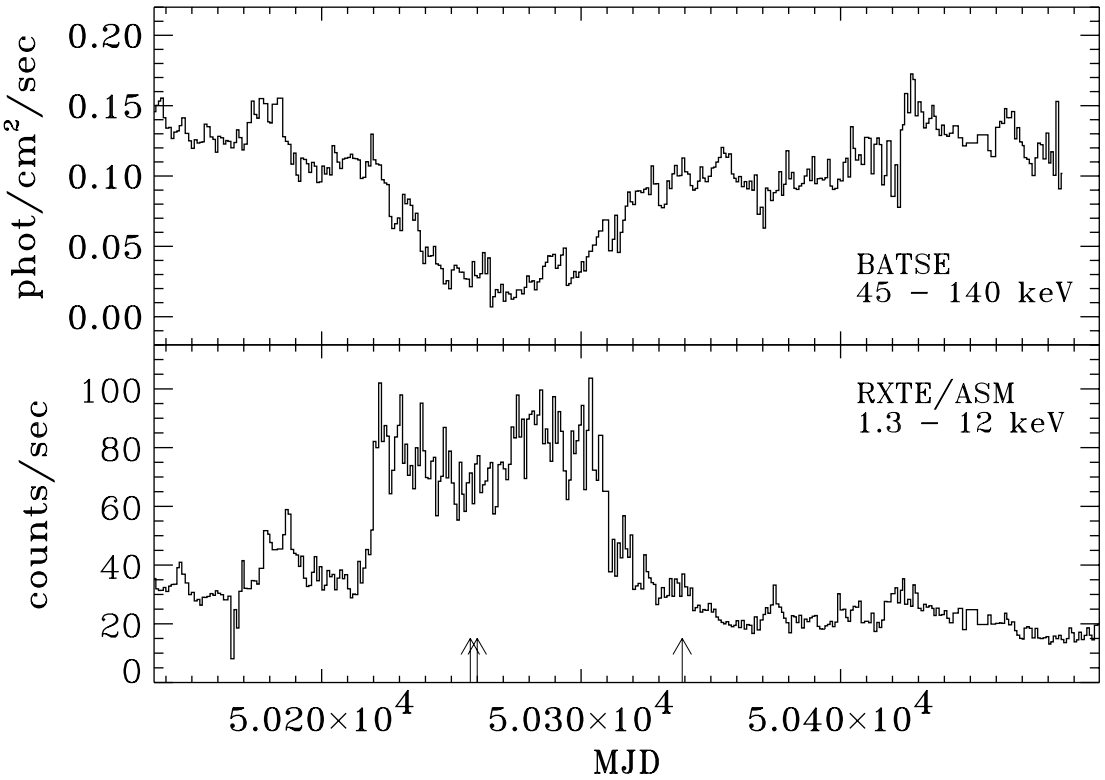

FIG. 1.—One-day–average light curve of Cyg X-1 detected with the *CGRO*/BATSE and *RXTE*/ASM during the 1996 state transitions. (From the public archives at cossc.gsfc.nasa.gov/batse/hilev/occ.html and xte.mit.edu/XTE/asmlc/ASM.html, respectively.) *BeppoSAX* observations are indicated with arrows.

inner radius of the disk and a power law with $\Gamma = 2.15 \pm 0.02$. The February spectrum was fit with a power law with $\Gamma = 1.60 \pm 0.02$, a Fe K line, and an edge. Dotani et al. (1997) reported results of an *ASCA* observation (0.5–10 keV) performed on 1996 May 30–31. The lower energy part of the spectrum (0.5–4.5 keV) was fit by either the "multicolor" disk model with inner temperature of $kT_{\rm in} = 0.43$ keV or by a general relativistic blackbody disk model (Hanawa 1989). The higher energy spectrum (4.5–10 keV) was accounted for a power law ($\Gamma = 2.3 \pm 0.1$) and a "smeared edge" model. Combining the *ASCA* observation with the simultaneous *RXTE* observation, Cui et al. (1998) fit the 0.7–50 keV spectrum with a model consisting of "multicolor" blackbody, thermal Comptonization with electrons at $kT \simeq 40$ keV, Compton reflection, and a broad Fe Kα line feature (with a Gaussian width of $\sim$0.35 keV and an equivalent width of $\sim$130 eV). However, physical interpretation of the results is rather unclear because the temperature of the seed photons for Comptonization was more than twice the maximum disk blackbody temperature.

The simultaneous *ASCA*/*RXTE* data were also considered by G99. They found that thermal Comptonization at 40 keV (as obtained by Cui et al. 1998) was unable to reproduce the *Compton Gamma Ray Observatory* (*CGRO*) OSSE data (of 1996 June 14–25), with a power law with $\Gamma \sim 2.5$ extending to $\gtrsim$600 keV without a cutoff. An increase of the plasma temperature could improve the fit at high energies but would strongly worsen the disagreement with the data below $\sim$10 keV (see also Coppi 1999). Furthermore, thermal-Compton models in which the source of seed photons for upscattering was the disk emission were completely unacceptable even for the *RXTE*/*ASCA* data alone. Thus, G99 concluded that the thermal-Compton model for the SS can be rejected.

An alternative model found by G99 to fit well the *ASCA*/*RXTE*/OSSE data was that of a nonthermal plasma (with electron acceleration) located in the vicinity of the accretion disk, possibly forming a corona. In steady state, the electron distribution is hybrid, containing both thermal and nonthermal components, and both components Compton upscatter the disk emission. The specific model is developed from a code by Coppi (1992).

In this work, we study two sets of observations of Cyg X-1 performed by *BeppoSAX* in 1996. During the first set, the source was in the SS. During the second one, it was already back in its HS, based on its spectral properties as determined by the *RXTE* All-Sky Monitor (VASM; Wen, Cui, & Bradt 2000). The X-ray spectrum during that observation is softer than that measured by G97 but similarly soft spectra are commonly seen by the ASM during the HS. In fact, our second observation corresponds to about the middle of the region covered by the ASM data on a color/intensity diagram during the hard state (Zdziarski, Wen, & Paciesas, 2000, in preparation). Furthermore, it appears to fall after the periods of enhanced time lags characteristic to state transitions in Cyg X-1 (Pottschmidt et al. 2000).

Unlike other missions, *BeppoSAX* offers the possibility to cover a wide energy band (0.1–300 keV), which is crucial to constrain models. Moreover, we can compare the spectra obtained with the same instruments in different states. Preliminary results of spectral analysis of the observations were reported by Palazzi et al. (1999). In § 2 below, we describe the observations and discuss time variability of our data. In § 3, we describe our method of spectral analysis, and its

results are given in § 4. Finally, in § 5, astrophysical consequences of our results are discussed.

2. OBSERVATIONS, DATA SETS, AND TIMING

The *BeppoSAX* payload includes four Narrow Field Instruments (NFIs, Boella et al. 1997a), which embody a Low-Energy Concentrator Spectrometer (LECS, 0.1–10 keV, Parmar et al. 1997), three Medium-Energy Concentrators Spectrometers (MECS, 1.3–10 keV, Boella et al. 1997b), a High-Pressure Gas Scintillator Proportional Counter (HPGSPC, 3–100 keV, Manzo et al. 1997), and a Phoswich Detection System (PDS, 15–300 keV, Frontera et al. 1997). Both LECS and MECS have imaging capabilities, while the HPGSPC and PDS are direct-viewing detectors with a Field of View (FOV) of 1° and 1°.3, respectively. The latter instruments use rocking collimators for background monitoring.

The first Cyg X-1 observation (obs. 1) was performed on 1996 June 22 (first light of *BeppoSAX*). The source was offset by about 14′ with respect to the instrument axes, as established from the MECS image. The source was observed again on-axis (obs. 2) on 1996 June 25. Unfortunately, in this observation, only the MECS were switched on. Other observations were performed in 1996 September 12–13 with all the NFIs operative. These observations were devoted to a diagonal scan of the NFI field of view to assess their off-axis response. Two of them (obs. 3A and 3B) were almost on axis (offset less than 3′). The log of the observations is given in Table 1, together with the phase of the 5.6 d binary orbit with respect to the superior conjunction of the X-ray source (using the ephemeris of Brocksopp et al. 1999).

Useful data from obs. 1, obs. 2, and obs. 3 were selected from time intervals that met the following criteria: satellite outside the South Atlantic Geomagnetic Anomaly, the elevation angle above the Earth limb of $\geq 5°$, dark Earth (for LECS), stabilized high voltage supplies. For obs. 1, the MECS data were not usable for spectral analysis because the centroid of the image coincided with the strong-back of the detector entrance window, which introduced a complex spatial modulation of the window transparency.

The LECS and MECS source spectra were extracted from regions with radii of 8′ and 7′, respectively, around the centroid of the source image. We used as background spectrum that obtained from the observation of blank fields. The spectra from the three MECS units were equalized and co-added. For obs. 2, we analyzed only data from MECS units 2 and 3 since the data files of the unit 1 at the epoch of this observation were corrupted. The background levels of HPGSPC and PDS were estimated by swapping their collimators every 96 s. During obs. 3A, the detectors were continuously pointed at the source, so the background level was not available for this observation. Therefore, for the broadband spectral analysis we used obs. 3B, during which the background was continuously monitored.

Although our paper deals primarily with spectral analysis, we also have performed some temporal analysis of our data. Specifically, we have obtained the cross-correlation function between the light curves in two bands of the MECS detector, soft, 1.3–4 keV, and hard, 4–10 keV, in the two spectral states. The cross-correlation was computed using a fast Fourier transform (FFT) algorithm (under XRONOS) for the time series binned at the time resolution of 100, 10, and 1 ms. We have found that the cross-correlation function does not depend on the binning, and we have detected no measurable time lags, in agreement with the results of an analysis of the *RXTE*/PCA data by Maccarone, Coppi, & Poutanen (2000). Note that the *BeppoSAX* detectors are much less sensitive than those of the *RXTE*/PCA, which remains the primary tool for this kind of analysis.

Then, we have considered the possible spectral variability of the source. We have found that the light curves integrated over 200 s show a source time variability up to $\sim 30\%$ on timescale of several hundred seconds. We have tested for obs. 3A the spectral variability by subdividing that observation into three segments of $\sim 10^4$ s each. No statistically significant variation of the best-fit parameters from one segment to another was found. Thus, below we consider the spectra averaged over each observation.

3. SPECTRAL ANALYSIS

The count rate spectra were analyzed using the XSPEC version 10 software package (Arnaud 1996). The adopted response matrices took into account the offset, if any, of the observed source centroid. Intercalibration analysis of the

TABLE 1

THE OBSERVATION LOG

Observation Number	Date	Start Time	End Time	Orbital Phase	Instrument	Exposure (s)
1	1996 Jun 22	18:33:21	20:05:18	0.93–0.94	LECS	844
	...	...	...	...	MECS[a]	2328
	...	...	...	...	HPGSPC	750
	...	...	...	...	PDS	1480
2	1996 Jun 25	09:03:15	13:40:05	0.40–0.43	MECS	7461
3A	1996 Sep 12	00:52:00	11:09:50	0.51–0.52	LECS	4641
	...	...	...	...	MECS	19653
	...	...	...	...	HPGSPC[b]	8845
	...	...	...	...	PDS[b]	10560
3B	1996 Sep 12	11:10:11	15:44:50	0.52–0.55	LECS	150
	...	...	...	...	MECS	8915
	...	...	...	...	HPGSPC	7863
	...	...	...	...	PDS	2844

[a] Unusable because of the offset of 14′ of the source from the instrument axis.
[b] Unusable because of no available background.

BeppoSAX NFIs using Crab Nebula (Fiore, Guainazzi, & Grandi 1999)[10] has shown that systematic uncertainties in the spectrum determination are $\sim 1.5\%$. To limit these systematic errors in the deconvolved spectra, the energy band of each instrument was limited to that where the response function was best known: LECS, 0.5–4 keV; MECS, 3–10 keV; HPGSPC, 5–40 keV; PDS, 15–200 keV. However, for obs. 1, where the MECS data are not available, we used 0.5–5 keV and 5–25 keV for the LECS and HPGSPC, respectively. We allowed for free normalization of the instruments in multi-instrument fits with respect to MECS in the HS (§ 4.2) and the LECS in the SS (§ 4.3). For clarity of display, the spectra from multi-instrument fits shown in Figures 3, 5 below were renormalized to the level of the MECS and LECS, respectively.

The quoted errors for the spectral parameters correspond to a 90% confidence level ($\Delta\chi^2 = 2.71$). Parameters in brackets in tables below were fixed during fits. In modeling absorption and reflection, we assume the abundances of Anders & Ebihara (1982) and, following G99, the disk inclination of $i = 45°$.

4. RESULTS

4.1. *Simple Models to the LECS and MECS Spectra*

During the SS (obs. 2), the mean 2–10 keV flux level of the source was 1.7×10^{-8} ergs cm^{-2} s^{-1}, while during the HS (obs. 3A), the corresponding flux was 7.9×10^{-9} ergs cm^{-2} s^{-1}, i.e., lower by a factor of 2. Our HS flux is higher than that typically measured in the HS by *ASCA*, $\sim 5 \times 10^{-9}$ ergs cm^{-2} s^{-1} (E96), but it is similar, e.g., to the HS value of 7.5×10^{-9} ergs cm^{-2} s^{-1} obtained for observation 2 of G97.

We find that the energy range of each single NFI instrument is too narrow to constrain physical models in either of the observed states. A sum of a power law (PL) and a blackbody (BB) photoabsorbed by a hydrogen column density, $N_{\rm H}$, provides an acceptable fit (the reduced $\chi^2/\nu = 376/321$) to the LECS (0.5–4 keV) continuum during the HS (obs. 3A). The same model provides a very good fit ($\chi^2/\nu = 311/321$) to the corresponding spectrum measured during the SS (obs. 1). In Table 2, we summarize the results. As can be seen, we find a statistically significant higher value of the BB temperature in the SS, $kT_{\rm bb} \simeq 0.30$ keV, than $kT_{\rm bb} \simeq 0.18$ keV found in the HS. Also, the PL slope is higher in the SS, with the photon index of $\Gamma \simeq 2.8$, while $\Gamma \simeq 2.2$ in the HS. Figure 2 compares the strength of the blackbody component in the HS and the SS. The higher amplitude and temperature of the blackbody in the SS are apparent. The hydrogen column density does not appear to significantly change from obs. 1 to obs. 3A and, thus, also with the orbital phase (see Table 1) of the binary period of Cyg X-1. This item will be discussed later (§ 5.4).

TABLE 2

PARAMETERS OF THE BLACKBODY + POWER-LAW MODEL FOR THE LECS 0.5–4 keV RANGE

Parameter	HS (obs. 3A)	SS (obs. 1)
$N_{\rm H}$ (10^{21} cm^{-2})	5.4 ± 0.3	5.9 ± 0.4
Γ	2.15 ± 0.03	2.80 ± 0.15
$F_{\rm PL}$(1 keV) (cm^{-2} s^{-1}).....	4.69 ± 0.04	17^{+17}_{-11}
$kT_{\rm bb}$ (keV).....	0.184 ± 0.006	0.30 ± 0.01
$L_{\rm bb}$ (10^{37} ergs s^{-1}).....	0.44 ± 0.04	2.3 ± 0.4
$R_{\rm bb}$ (km)	170 ± 14	147 ± 15
χ^2/ν	376/321	311/321

[10] Fiore, F., Guainazzi, M., & Grandi, P. 1999, Cookbook for *BeppoSAX* NFI Spectral Analysis can be found at http://www.sdc.asi.it/software/cookbook.

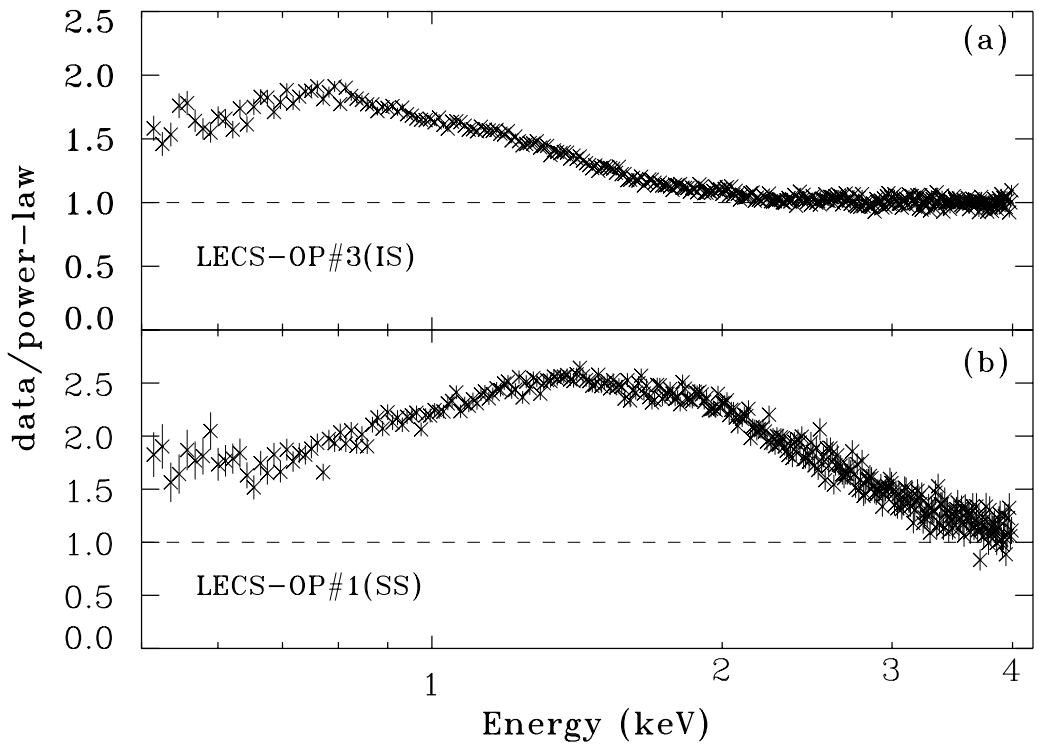

FIG. 2.—Ratio of the LECS spectrum to the best-fitting power-law model component (see Table 2) during the HS (*a*) and the SS (*b*)

A simple model (BB+PL) for the continuum plus a broad Gaussian line (with the peak energy, width, and photon flux of $E_{\rm Fe}$, $\sigma_{\rm Fe}$, and $I_{\rm Fe}$, respectively) also provides a good fit ($\chi^2/\nu = 160/143$) to the 3–10 keV spectrum measured by the MECS during the SS (obs. 2). We have also checked the effect of replacing the Gaussian line by a disk line (DL) model of Fabian et al. (1989) with rest-frame energy $E_{\rm Fe}$ and flux of $I_{\rm Fe}$, with the disk emitting the line from a radius, $R_{\rm out}$, down to $R_{\rm in} \geq 6R_{\rm g}$ (where $R_{\rm g} \equiv GM/c^2$) with the surface emissivity dependence $\propto R^{-2}$. We have found that the χ^2/ν somewhat improves (150/146) for the inclination of $i = 60°$, but it gets significantly higher (199/146) for $i = 45°$. However, this worsening of the fit for $i = 45°$ is no longer present in our physical model (§ 4.3). The best-fit continuum parameters and the line parameters for both models are reported in Table 3. Notice that the BB temperature estimated with MECS from obs. 2 is slightly higher than that obtained with LECS in obs. 1. Given the MECS energy band, this higher value is likely biased, and we consider the LECS result more reliable. The values of Γ estimated from obs. 1 and obs. 2 are instead completely consistent within each other.

The BB+PL continuum model plus a Gaussian provides a marginally acceptable fit also to the MECS 3–10 keV data in the HS (obs. 3A, see Table 3). The DL profile provides a fit as good as the Gaussian. The best-fit parameters of the line are consistent with those obtained during the SS, except the line equivalent width (EW), which is lower during the HS. The BB luminosity is poorly constrained by the 3–10 keV data in the HS.

On the other hand, we find that simple models fail to describe the broad band, 0.5–200 keV, spectra of obs. 1 and obs. 3B. One can describe those data in terms of Comptonization, blackbody emission, Compton reflection, and Fe Kα fluorescence; see § 4.2 below.

4.2. *Physical Model for the 0.5–200 keV Spectrum of the Hard State*

A power law, with Compton reflection and a Fe K line, was found suitable to describe the HS spectrum up to 20 keV (Palazzi et al. 1999). However, a simple assumption of an exponential cutoff in the power law was insufficient to describe the spectrum above 20 keV. Thus, we have investigated whether replacing the *e*-folded power law by a spectrum from Comptonization can provide a satisfactory description of the broadband spectrum. We have found, however, that none of an extensive array of models by either Poutanen & Svensson (1996) or Haardt (1993) for various geometries can, even approximately, describe the actual data (obs. 3B).

On the other hand, we could obtain satisfactory fits constraining the energy ranges either below or above $\sim$10 keV. This provided us a motivation to consider models with two Comptonizing regions, which are likely to provide a better approximation to the actual X-ray source in Cyg X-1. In support of this scenario, G97 found that two thermal-Comptonization components were required to account for the *Ginga*/OSSE hard-state data of Cyg X-1.

Thus, we have considered a model containing two thermal-Comptonization spectra, corresponding to different temperatures kT_1 and kT_2, and the Thomson optical depths, τ_1 and τ_2. For simplicity and to minimize the number of free parameters, we have assumed that each of the Comptonization sources can be represented by emission of a spherical plasma cloud with a uniform distribution of seed blackbody photons (with τ measured along the radius). We used the model COMPPS, version 3.4[11] (Poutanen & Svensson 1996). As independent parameters, we choose kT_1, kT_2, and the Compton parameters y_1 and y_2, where

$$y_i \equiv 4\tau_i \frac{kT_i}{m_{\rm e}c^2}\,, \qquad (1)$$

and $i = 1, 2$. This choice allows us to distinguish the spectral hardness of the two components since a given value of y corresponds to an approximately constant value of Γ (e.g., Ghisellini & Haardt 1994; Poutanen 1998; Beloborodov 1999b).

The present data are not able to constrain $N_{\rm H}$ with our model. Therefore, it was fixed at the best-fit value obtained using the SS (see § 4.3). Furthermore, the data do not allow us to distinguish between rather similar components from Compton reflection of the emission of the two plasma clouds. (For this process, we use Green's functions of Magdziarz & Zdziarski 1995.) Therefore, we have exploited here a

[11] The COMPPS code is available on the internet at ftp://ftp.astro.su.se/pub/juri/XSPEC/COMPPS.

TABLE 3

PARAMETERS OF THE BLACKBODY + POWER-LAW + LINE MODEL FOR THE MECS 3–10 keV RANGE

	GAUSSIAN LINE		DISK LINE	
PARAMETER	HS (obs. 3A)	SS (obs. 2)	HS (obs. 3A)	SS (obs. 2)
$N_{\rm H}$ (10^{21} cm^{-2})	[6.0]	[6.0]	[6.0]	[6.0]
Γ	1.90 ± 0.02	2.78 ± 0.03	1.89 ± 0.01	2.70 ± 0.03
$F_{\rm PL}$ (1 keV) (cm^{-2} s^{-1})	2.82 ± 0.10	10.5 ± 0.6	2.75 ± 0.08	9.1 ± 0.6
$kT_{\rm bb}$ (keV)	0.276 ± 0.1	0.36 ± 0.01	0.30 ± 0.07	0.37 ± 0.01
$L_{\rm bb}$ (10^{37} ergs s^{-1})	$0.4^{+3.6}_{-0.3}$	1.7 ± 0.2	$0.3^{+1.2}_{-0.2}$	1.64 ± 0.12
$E_{\rm Fe}$ (keV)	6.43 ± 0.10	6.54 ± 0.04	[6.4]	[6.4]
$\sigma_{\rm Fe}$ (keV)	0.68 ± 0.16	0.65 ± 0.09	...	...
$I_{\rm Fe}$ (10^{-2} cm^{-2} s^{-1})	1.2 ± 0.3	1.65 ± 0.27	1.08 ± 0.14	1.55 ± 0.15
EW (eV)	146 ± 40	300 ± 50	146 ± 20	300 ± 30
$R_{\rm in}/R_{\rm g}$	...	...	10^{+5}_{-4}	6^{+4}
$R_{\rm out}/R_{\rm g}$	...	...	100^{+90}_{-40}	100^{+50}_{-30}
i (deg)	...	...	[45]	[45]
χ^2/ν	175/143	160/143	169/143	199/143

correlation between the relative strength of Compton reflection, $\Omega/2\pi$, and Γ found in Cyg X-1 by Gilfanov, Churazov, & Revnivtsev (1999, hereafter GCR99). This correlation is also present in other black-hole binaries as well as in Seyfert 1 galaxies (Zdziarski, Lubiński, & Smith 1999). According to it, the softer the spectrum, the larger the value of $\Omega/2\pi$. To take into account this effect, we have assumed that $\Omega/2\pi$ of the softer component is twice that of the harder component. The seed photons for Comptonization are assumed to have a blackbody distribution with a temperature $kT_{\rm bb}$.

This model does indeed provide a good description of the data (see Table 4). From equation (1), the optical depths corresponding to the fitted values of y of the soft and hard Comptonization components are $\tau_1 = 0.5 \pm 0.2$ and $\tau_2 = 1.9 \pm 0.2$, respectively. No additional (i.e., not passing through the hot plasma) blackbody component is required by the fit, but its presence cannot be ruled out. We also find that replacing the blackbody distribution of the seed photons by that of a disk blackbody yields a fit worse by $\Delta\chi^2 = +6.3$.

Figure 3 compares the resulting model spectrum with the data. We see that the hard component dominates at energies $\gtrsim 1.5$ keV, with the soft one providing a soft excess, dominant at lower energies. The temperature of the soft component is thus weakly constrained because of its small contribution to the spectrum around the high-energy cutoff. Compton reflection is dominated by that of the harder component, with $\Omega_2/2\pi = 0.25 \pm 0.04$.

In addition to the continuum, a strong and broad line is also present in the spectrum. The residuals of the data to the continuum model are shown in Figure 4. The line and edge region are much better fitted by static reflection and a Gaussian ($\chi^2/\nu = 377/361$—see Table 4) than by the line and reflection coming from a disk. In the latter case, best fits have been obtained for the radial dependence of the line and reflection being the same as that of the disk emission itself. Still, the obtained fits are much worse than that of Table 4, $\chi^2/\nu = 469/362$ and 451/362 for $i = 45°$ and 60°, respectively. At $i = 60°$, EW = 190 eV and $\Omega_2/2\pi = 0.42$.

The total unabsorbed 0.5–200 keV flux and the bolometric flux derived from our model are 4.2×10^{-8} ergs cm^{-2} s^{-1} and 5.1×10^{-8} ergs cm^{-2} s^{-1} (corresponding to the luminosities of $\sim 2.0 \times 10^{37}$ and 2.4×10^{37} ergs s^{-1} at $d = 2$ kpc and assuming isotropy), respectively. The bolometric fluxes in the hard and soft components are 3.5×10^{-8} ergs cm^{-2} s^{-1} and 1.6×10^{-8} ergs cm^{-2} s^{-1}, respectively.

TABLE 4

PARAMETERS OF THE THERMAL-COMPTON MODEL FOR THE 0.5–200 keV HARD STATE SPECTRUM (OBS. 3B)

Parameter	Value
$N_{\rm H}$ (10^{21} cm^{-2})	[6.0]
$kT_{\rm bb}$ (keV)	0.16 ± 0.02
kT_1 (keV)	42 ± 19
y_1	0.15 ± 0.01
F_1 (1 keV) (cm^{-2} s^{-1})	1.7 ± 0.8
kT_2 (keV)	59 ± 5
y_2	0.89 ± 0.01
$\Omega_2/2\pi$	0.25 ± 0.04
F_2 (1 keV) (cm^{-2} s^{-1})	1.55 ± 0.09
$E_{\rm Fe}$ (keV)	6.15 ± 0.12
$\sigma_{\rm Fe}$ (keV)	1.22 ± 0.13
$I_{\rm Fe}$ (10^{-2} cm^{-2} s^{-1})	2.71 ± 0.43
EW (eV)	350 ± 55
χ^2/ν	377/361

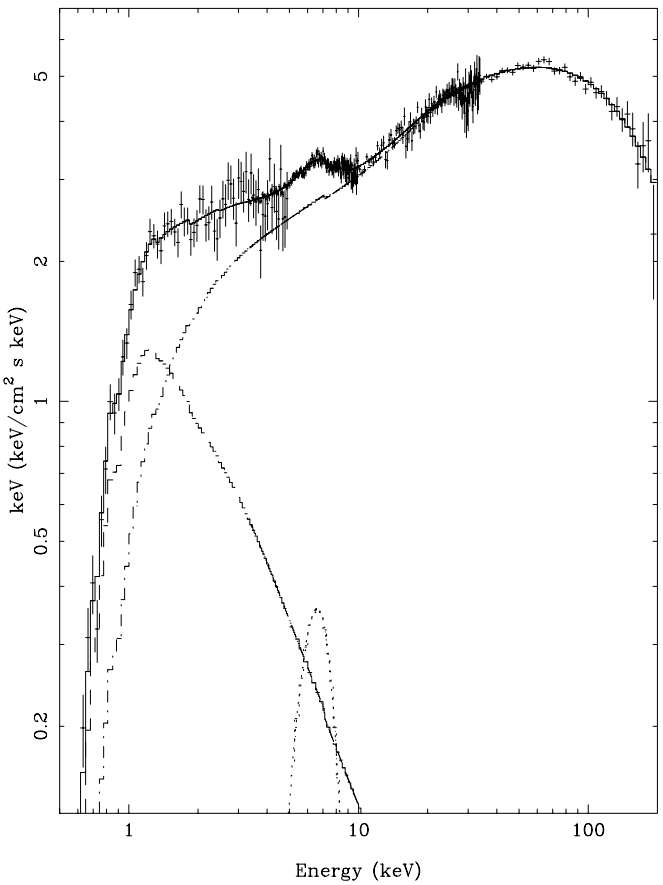

FIG. 3.—Broadband EF_E spectrum during the HS (crosses). Histograms show the model components caused by two thermal-Compton plasmas with Compton reflection and a broad Gaussian (see § 4.2 and Table 4).

4.3. *Physical Model for the 0.5–200 keV Spectrum in the Soft State*

The above thermal-Comptonization model does not fit the SS spectrum. The reasons are the same as those given by G99 for the SS measured by *ASCA*/*RXTE* 1996 May 30 (which also took into account the OSSE data of 1996 June 14–25); namely, the presence of an extended power-law–like tail at high energies and of a soft excess. G99 have fitted their data by a nonthermal Comptonization model developed from a code of Coppi (1992; see also Poutanen & Coppi 1998).

The model is described in G99, where we refer the reader for details. Its main ingredient is a hot plasma cloud with continuous acceleration of electrons at a rate $\propto \gamma^{-\Gamma_{\rm inj}}$. The high-energy electrons lose energy because of Compton, Coulomb, and bremsstrahlung processes and thus establish a steady-state distribution. At high energies, the distribution is nonthermal (power-law like), but at low energies a Maxwellian distribution is established. The temperature of the Maxwellian, $kT_{\rm e}$, is determined by balance between Compton gains and losses, Coulomb heating by high-energy electrons, bremsstrahlung losses, and a direct heating (e.g., Coulomb heating by energetic ions). The total number of Maxwellian electrons (not including $e^{\pm}$ pairs, the

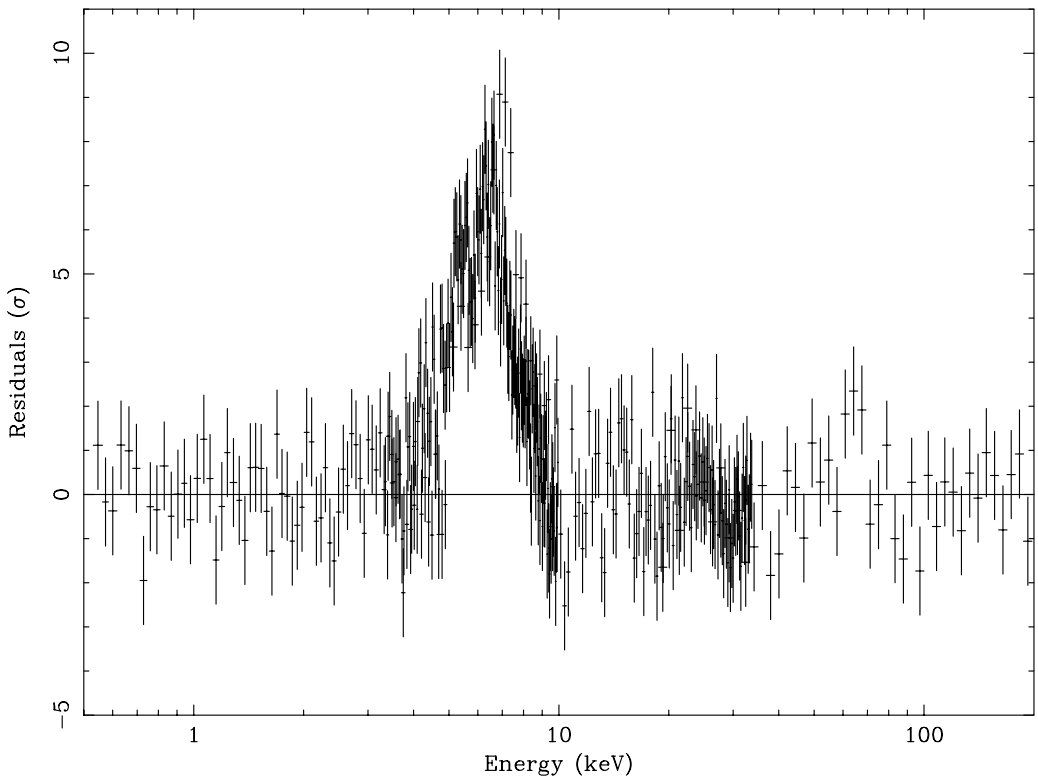

FIG. 4.—Ratio of the HS data to the best-fit continuum model (Fig. 3 and Table 4) excluding the Fe Kα line, which large width is apparent

production of which is also taken into account) is determined by the corresponding Thomson optical depth, τ_i (the second free parameter). The cloud is irradiated by blackbody photons emitted by an accretion disk. These photons serve as seed for Compton scattering by both thermal and nonthermal electrons.

The system is characterized by powers, L_i, supplied to its different components. We express each of them dimensionlessly as a compactness, $\ell_i \equiv L_i \sigma_T/(\mathcal{R} m_e c^3)$; $\mathcal{R}$ is the characteristic dimension of the plasma and σ_T is the Thomson cross section. ℓ_s, ℓ_{th}, ℓ_{nth}, and $\ell_h = \ell_{th} + \ell_{nth}$ correspond to the power in soft disk photons irradiating the plasma, in direct electron heating, in electron acceleration, and total power supplied to electrons in the plasma, respectively. As found by G99, the fits allow a range of ℓ_s, in which the dominant energy-loss process of energetic electrons is Compton, and $e^{\pm}$ pair production does not yield a visible annihilation feature (not seen in the OSSE data). Following G99, we fix here $\ell_s = 10$.

The disk spectrum incident on the plasma is modeled as coming from a pseudo-Newtonian accretion disk extending from infinity down to the minimum stable orbit, $R_{in} = 6R_g$, the spectral shape of which can be characterized by the maximum color temperature of the disk, kT_{max}. The spectrum from both reflection and the Fe Kα fluorescence is calculated, taking into account relativistic smearing with $R_{out} = 10^3 R_g$, R_{in} as above, and the emissivity dependence $\propto R^{-2}$ (see § 4.1). The reflected surface is allowed to be ionized, with the degree of ionization characterized by the ionization parameter $\xi \equiv 4\pi F_{ion}/n$ (where F_{ion} is the ionizing flux and n is the reflector density).

The fit does not change with the disk inclination ($\chi^2/\nu = 167.9/184$, 167.1/184 for $i = 45°$, 60°, respectively). The best-fit parameters for $i = 45°$ are given in Table 5, which, for comparison, also shows the results of G99. Figure 5 shows the observed broadband spectrum as well as the model and its components. Note that we find a lower disk ionization than that in the observation of G99.

The 0.5–200 keV and bolometric unabsorbed fluxes (normalized to the LECS) are 1.0×10^{-7} ergs cm^{-2} s^{-1} and 1.5×10^{-7} ergs cm^{-2} s^{-1} ($L \simeq 7.1 \times 10^{37}$ ergs s^{-1} assuming isotropy), respectively. They are higher by a factor of ~ 3 than those in the HS. The main change in the flux is in the 0.5–2 keV range, where the blackbody photon flux is more prominent; 1.3×10^{-8} ergs cm^{-2} s^{-1} in the HS versus 7.7×10^{-8} ergs cm^{-2} s^{-1} in the SS.

So far, we have modeled the Fe Kα line as coming from a disk extending down to $R_{in} = 6R_g$. When we relax this assumption, we obtain $R_{in} = 6^{+5}_{0} R_g$. Alternatively, the line can be described as a Gaussian, with $\chi^2/\nu = 165/183$, very

TABLE 5

PARAMETERS OF THE HYBRID MODEL FOR THE 0.5–200 keV SOFT STATE SPECTRUM (OBS. 1)

Parameter	*BeppoSAX* (June 22)	*ASCA*/*RXTE* (May 30)
N_H (10^{21} cm^{-2})	6.0 ± 0.1	$5.2^{+0.1}_{-0.2}$
kT_{max} (keV)	0.368 ± 0.006	$0.36^{+0.01}_{-0.01}$
ℓ_h/ℓ_s	$0.168^{+0.015}_{-0.020}$	$0.35^{+0.01}_{-0.02}$
ℓ_{nth}/ℓ_h	0.6 ± 0.20	$0.77^{+0.05}_{-0.04}$
τ_i	$0.098^{+0.016}_{-0.012}$	$0.25^{+0.05}_{-0.04}$
Γ_{inj}	2.4 ± 0.2	$2.54^{+0.11}_{-0.07}$
$\Omega/2\pi$	$1.5^{+1.4}_{-0.6}$	$0.63^{+0.13}_{-0.11}$
ξ (ergs cm s^{-1})	65^{+33}_{-23}	350^{+250}_{-120}
E_{Fe} (keV)	[6.4]	$6.37^{+0.14}_{-0.14}$
EW (eV)	80 ± 60	120^{+50}_{-30}
χ^2/ν	167.9/184	618/574

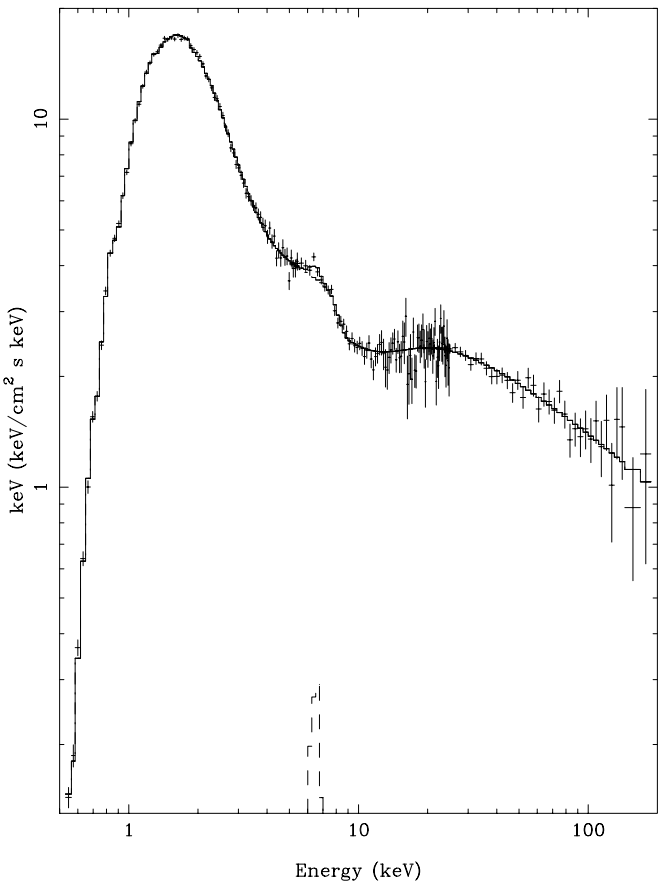

FIG. 5.—Broadband EF_E spectrum during the SS (*crosses*). Histograms show the continuum model with the hybrid plasma Compton upscattering blackbody disk photons and a broad disk line.

similar to the disk-line case. Then, $E_{\rm Fe} = 6.2 \pm 0.3$ keV and $\sigma_{\rm Fe} = 0.4 \pm 0.4$ keV.

We notice that the (single-component) hybrid model is not suitable to describe the 0.5–200 keV HS spectrum. Even if we restrict the energy band to 4–200 keV, which is dominated by the hard Comptonization component in our spectrum, we find a rather unsatisfactory fit ($\chi^2/\nu = 374/281$) corresponding to a probability of only 1.6×10^{-4} that this model is correct. This shows that the spectrum observed by us (belonging to the HS, see § 1) is different from the spectra observed by *RXTE* during the spectral transition on 1996 May 22–23, which were successfully fitted by G99 with the hybrid model in the same energy range.

5. DISCUSSION

5.1. *Accretion Flow in the Hard State*

One of our main new results is the interpretation of the soft excess in the HS state as being caused by thermal Comptonization by a hot plasma with a low value of the Compton parameter (y), whereas the main, hard X-ray continuum is caused by thermal Comptonization by a plasma with a higher y. Our model with two plasma components represents, most likely, an approximation of a spatial distribution of the temperature and optical depth with radius.

This result appears to apply to the HS in general, with a soft excess at $\lesssim 3$ keV being commonly found (E96, G97). In fact, a strong evidence for a radial stratification of the X-ray source in Cyg X-1 in the HS is provided by results of Fourier-frequency resolved spectroscopy (Revnivtsev, Gilfanov, & Churazov 1999; GCR99). These authors show that the total spectrum of Cyg X-1 contains components with different values of Γ corresponding to different frequency ranges of temporal variability.

Figure 3 shows that the hard component dominates at energies $\gtrsim 1.5$ keV and the bolometric emission (§ 4.2). This is, in fact, in agreement with the result of GCR99, who found that the time-averaged spectrum in the HS of Cyg X-1 is similar to the hardest of the frequency-resolved spectra (see their Fig. 8). This implies that the average spectrum is dominated by a hard component constant in time, similar to the situation in our model.

The temperature of the main, hard component, $kT \simeq 60$ keV, is less than that measured by G97 ($kT \sim 100$ keV). On the other hand, our value of kT is almost the same as that found in the HS of another persistent black-hole binary, GX 339−4 (Zdziarski et al. 1998). The temperature of our soft component is similar but not well constrained because of its small contribution at highest energies (see Fig. 3). The plasma emitting the soft component appears to be farther away from the black hole according to the decrease of the typical frequency of the intensity variations with Γ in the spectroscopy of Revnivtsev et al. (1999). This is also supported by our result that the Thomson optical depth of the softer component is much less than that of the hard one, in agreement with accretion disk models, the generic feature of which is an increase of τ inward. We note that our model of the soft excess is different from that in which the soft emission is attributed to Comptonization in a warm (with $kT \sim 1$ keV) surface layer above the accretion disk (e.g., Czerny & Elvis 1987; Zhang et al. 2000).

We note that our result that the line in the HS is broad agrees with results of Done & Życki (1999) for the HS, who found broad lines in their reanalysis of the *ASCA* and *EXOSAT* data, even though from previous studies of those data (Done et al. 1992; E96) the lines were found to be narrow. Also, broad lines were reported in the *RXTE* data (GCR99).

An important unresolved issue for our model is the strength of the Fe Kα line as compared with the strength of reflection (dominated by the hard component). Namely, as seen in Table 4, the relatively low reflection strength of $\Omega/2\pi \sim 0.25$ cannot explain the strong Fe Kα line with EW of ~ 350 eV (see, e.g., Życki & Czerny 1994). We feel that this disagreement is caused by our two-zone approximation for the incident continuum being insufficient to describe the actual distribution of plasma parameters. The strong dependence on the assumed continuum is shown by comparison with the results assuming relativistic smearing by a disk, in which case EW $\simeq 190$ eV and $\Omega/2\pi \simeq 0.42$ (§ 4.2) as well as with Table 3, in which we found EW $\simeq 150$ eV assuming a power-law continuum for the MECS data only. Furthermore, our finding that a Gaussian line fits the data better than the disk line (§ 4.2) probably indicates a distribution of the cold medium different from a disk, e.g., blobs embedded in a hot medium (Poutanen 1998; Zdziarski et al. 1998; Böttcher & Liang 1999) or an outflow.

In principle, it is possible that our obtained low value of the reflection strength is caused by heating and photoionization of a surface layer of the accretion disk (e.g., Nayakshin 2000; Nayakshin, Kazanas, & Kallman 2000). However, we find no signature of ionization in the data (the best-fit $\xi = 0$). Furthermore, the strength of reflection is

clearly higher in the SS, contrary to an expectation of that model that a much higher soft X-ray ionizing flux would reduce reflection even further.

We also note that the value of Ω is less than that expected on the basis of the $\Omega(\Gamma)$ correlation of GCR99. This appears to be, at least partly, caused by using different incident continuum models by us and by GCR99, who used spectra below 20 keV and the PEXRAV model of XSPEC for their fitting. In fact, our spectral data fitted below 20 keV with the same model (Palazzi et al. 1999) are in agreement with the correlation of GCR99.

5.2. *Accretion Flow in the Soft State*

Our results (§ 4.3) strongly confirm the applicability of the hybrid plasma model to the SS, as found by G99. Those authors present an exhaustive discussion of physical consequences of this model, which we thus do not repeat here. Most of the model parameters obtained by us and by G99 for their *ASCA*/*RXTE* observation are rather similar, as is shown in Table 5. However, when $R_{\rm in}$ is allowed to be free, G99 find its value as $17^{+26}_{-8}\,R_{\rm g}$, whereas we obtain $6^{+5}_{-0}\,R_{\rm g}$. This appears to indicate that the inner radius of the disk moved down to the minimum stable orbit between 1996 May 30 and June 22. This is also supported by the larger solid angle of the reflector obtained for the observation on June 22, $\Omega/2\pi = 1.5 \pm 0.6$ as compared with $0.63^{+0.13}_{-0.11}$ on May 30. Indeed, the temporal and spectral properties of Cyg X-1 on May 30 indicate the object was still undergoing a transition between the HS and SS (Cui et al. 1997; Pottschmidt et al. 2000; Wen et al. 2000).

We note that the EW of the Fe Kα line obtained by us, 80 ± 60 eV, is marginally too low for the strength of reflection with $\Omega/2\pi = 1.5 \pm 0.6$ (Życki & Czerny 1994). Given that our line profile relies on the data from HPGSPC (as MECS were not usable), we have also checked the EW of the line in obs. 2, when MECS were switched on. With the same continuum model, we found a similar value of the EW of 90 ± 40 eV. Still, the values of Ω and EW are consistent with each other within the 90% uncertainty ranges.

Other physical processes proposed to dominate in the SS are thermal Comptonization (e.g., Poutanen, Krolik, & Ryde 1997; Cui et al. 1998; Esin et al. 1998) and bulk-motion Comptonization (e.g., Laurent & Titarchuk 1999). Here, we have not been able to fit the *BeppoSAX* SS data with thermal Comptonization, confirming previous ruling out of this model (G99; Zdziarski 2000).

The bulk-motion Comptonization model is ruled out on the basis of the lack of a sharp high-energy cutoff at $\sim$100–200 keV (predicted by that model: Laurent & Titarchuk 1999) and the very large accretion rate required to account for the relatively hard power-law tail in the SS spectrum of Cyg X-1 (see Zdziarski 2000 for detailed discussion). We also note that McConnell et al. (2000) find a strong 1–10 MeV flux from Cyg X-1 in the SS observed by the *CGRO*/COMPTEL. That flux is completely inconsistent with the predictions of the bulk-Compton model. On the other hand, our best-fit hybrid model for the SS predicts no high-energy cutoff up to 10 MeV, and we find the predictions of that model for the 1–10 MeV range to be in agreement with the SS measurements of McConnell et al. (2000).

5.3. *The Nature of State Transitions*

In §§ 4.2–4.3, we have calculated that the bolometric fluxes (extrapolated from the 0.5–200 keV range using best-fitting models) in the HS and SS were $\sim 5 \times 10^{-8}$ ergs cm^{-2} s^{-1} and 1.5×10^{-7} ergs cm^{-2} s^{-1}, respectively. On the other hand, we have found that the bolometric flux during four observations of Cyg X-1 in 1991 in the HS by *Ginga* and OSSE (G97) was within the range of $\sim(3$–$6) \times 10^{-8}$ ergs cm^{-2} s^{-1}. The bolometric flux for the SS *ASCA*/*RXTE* data of G99 was 1.3×10^{-7} ergs cm^{-2} s^{-1} (normalized to the PCA). Thus, the bolometric flux measured by us in the two states appear typical. Our value of the bolometric flux in the SS is slightly higher than that found for the 1996 May 30 observation by G99, which may be caused by Cyg X-1 not yet having fully reached its SS during that observation.

Thus, we find that the increase of the bolometric flux in the SS with respect to that in the HS is by a factor of ~ 3. On the other hand, Zhang et al. (1997b) claimed the 1.3–200 keV flux remaining almost unchanged (within $\sim$15%) during transitions from the HS to SS, as well as constrained the change of the bolometric flux to be $\lesssim 1.5$. The disagreement between those results and ours probably stems from the uncertain relative calibration of the *RXTE*/ASM and *CGRO*/BATSE instruments used by Zhang et al. (1997b) and that the bulk of the flux in the HS and SS falls in the energy range of BATSE and ASM, respectively. On the other hand, we present here the flux measurements in the two states with the same instruments and with a broadband energy coverage.

If we assume isotropy, the (bolometric) luminosities in the HS and SS measured by us are $L = 0.016(d/2\ \mathrm{kpc})^2(M/10M_\odot)L_{\rm E}$ and $L = 0.048(d/2\ \mathrm{kpc})^2(M/10M_\odot)L_{\rm E}$, respectively. Here, $L_{\rm E} \equiv 4\pi\mu_e GMcm_p/\sigma_{\rm T}$ is the Eddington luminosity, $\sigma_{\rm T}$ is the Thomson cross section, $\mu_{\rm e} = 2/(1 + X)$ is the mean electron molecular weight, and $X \approx 0.7$ is the hydrogen mass fraction. For $X = 0.7$, $L_{\rm E} \simeq 1.48 \times 10^{38}(M/M_\odot)$ ergs s^{-1}.

However, the SS-to-HS luminosity ratio can be different than the flux ratio (G99, Beloborodov 1999a). One reason for that is that while the HS emission, coming mostly from an optically thin plasma, may be isotropic, the SS emission is predominantly caused by the anisotropic blackbody radiation. If $i < 60°$ (which is probably the case in Cyg X-1), the observed disk flux will be higher than that coming from an isotropic source with the same L. For the observations of G99 and $i = 35°$, the reduction of L because of this effect is by about $\frac{3}{4}$, which would correspondingly reduce the luminosity ratio between the SS and the HS. On the other hand, the hot plasma emission in the HS can be beamed toward the observer (Beloborodov 1999a), and thus anisotropic as well, in which case the luminosity ratio can be higher than the observed flux ratio.

The low relative reflection obtained during the HS (Table 4) would be in favor of a large inner radius of the accretion disk during this state. A large $R_{\rm in}$ is also in agreement with the BB flux and temperature lower than those in SS, but it is in conflict with the width, peak energy, and EW ($\sim$1.2 keV, $\sim$6.2 keV, and 350 eV, respectively) of the Fe Kα line observed during HS. On the other hand, the accretion flow in the SS is clearly dominated by an optically thick accretion disk extending down to the minimum stable orbit (§ 4.3).

Any theory of the state transition in Cyg X-1 has to take into account the above results. One possible cause of the transition is a change of $\dot{M}$. We note here that our above results on the SS-to-HS luminosity ratio being significantly

larger than the previously found value of $\lesssim 1.5$ (and likely as large as 3) make models based on the change of $\dot{M}$ much more plausible, as in now requiring much less fine-tuning.

The most detailed model postulating a change of $\dot{M}$ is probably that of Esin et al. (1998), in which the HS is very close to the maximum possible $\dot{M}$ of an optically thin advective flow (Narayan & Yi 1995; Abramowicz et al. 1995), and a further increase leads to a switch to accretion dominated by an optically thick accretion (Shakura & Sunyaev 1973). We note that the model in its original version postulated that an optically thick flow in the HS is truncated at $\gtrsim 10^3 R_g$. This appears to be in conflict with the Fe K line properties discussed above and the relativistic smearing also observed in the HS state (Done & Życki 1999). Also, another important modification required in that model is that the corona above the disk in the SS has to be nonthermal.

A related model attributes the state transitions to evaporation of the inner disk, which physical process occurs at a low $\dot{M}$ (Meyer, Liu, & Meyer-Hofmeister 2000; Różańska & Czerny 2000). Thus, the innermost flow in the HS consists of a hot plasma only. Then, a cold accretion disk with and without a hot corona exists at intermediate and large radii, respectively. The Fe Kα line is then formed at the intermediate radii. In the SS, the cold accretion disk extends down to the minimum stable orbit.

Beloborodov (1999a) has proposed that the source in the HS does not form an advective hot disk but, rather, a mildly relativistic outflow above the surface of an optically thick disk. The HS-to-SS transition would then involve the corona becoming static as well as nonthermal. The data studied here appear not to allow distinguishing between these possibilities.

Finally, Zhang, Cui, & Chen (1997a) have proposed that the Cyg X-1 state transition is caused by reversal of the direction of disk rotation from retrograde (HS) to prograde with the black hole spinning with an angular momentum of 0.75 GM c^{-1}. Disk reversals are possible from accretion fluctuations in stellar wind (Shapiro & Lightman 1976). Even if the transition to the HS was not terminated during our observations, some of the consequences discussed by Zhang, Cui, & Chen (1997a) could be in agreement with our results and with the observed variation of the total X-ray luminosity of Cyg X-1 during transition from SS to HS. However, this model has several difficulties. One is that the state transition in Cyg X- 1, accreting from a focused wind, should be caused by something different than the state transition in low-mass X-ray binaries, accreting from a Roche-lobe overflow. Then, it is unclear why the focused-wind accretion should be preferentially retrograde (with Cyg X-1 spending $\sim 90\%$ of time in the HS). We also note that the relationship between emission of the hot plasma and of the cold disk in the two states remains unexplained in this model.

5.4. *Hydrogen Column Density*

The hydrogen column density does not appear to significantly change with the source spectral state in our observations. Using the BB + PL model for the LECS data alone (Table 2) in the HS and SS, we find $N_H = (5.4 \pm 0.3)$ and $(5.9 \pm 0.4) \times 10^{21}$ cm^{-2}, respectively. The latter value fully agrees with that obtained using the hybrid Compton model for the SS broadband spectrum (§ 4.3), $(6.0 \pm 0.1) \times 10^{21}$ cm^{-2}.

We can compare those results with those based on the reddening of the system, which has been measured as $E(B-V) = 1.12 \pm 0.05$ (Bregman et al. 1973) and 0.95 ± 0.07 (Wu et al. 1982). The two values were obtained by averaging the reddening over regions centered on Cyg X-1 with the sizes of 30′ and 7°, respectively. No variation of the reddening with the orbital phase of the binary system was found (Wu et al. 1982). From the most extended all-sky study of the distribution of neutral H based on high-resolution *IUE* observations of Lyα absorption toward 554 OB stars, it has been found that their N_H is well correlated with the column density of dust, measured by $E(B-V)$, with $\langle N_H/E(B-V)\rangle = 4.93 \times 10^{21}$ cm^{-2} mag^{-1} (Diplas & Savage 1994). This implies $N_H = (5.5 \pm 0.2) \times 10^{21}$ cm^{-2} and $(4.7 \pm 0.3) \times 10^{21}$ cm^{-2} for the estimates of the extinction of Bregman et al. (1973) and Wu et al. (1982), respectively.

Our values of N_H, unlike the estimates based on the reddening, are also sensitive to the effect of absorption by circumstellar matter within the system, in which accretion proceeds via a focused wind from the companion. The wind is partially ionized and its observed column depends on the orbital phase, which leads to a modulation of the X-ray flux with the phase, discovered in the ASM data by Wen et al. (1999). Thus, we could have expected a significant difference between N_H in our HS observations (phase 0.51–0.55) and the SS one (phase 0.93–0.94). However, Wen et al. (1999) have found that the modulation becomes much weaker in the SS, which is, most likely, explained by the stronger ionization of the wind by the stronger soft X-ray flux in that state. This can explain our value of N_H at the phase ~ 0 in the SS being compatible with the value at the phase ~ 0.5 in the HS. Furthermore, Bałucińska-Church et al. (2000) have attributed the modulation to the effects of blobs of neutral matter causing the X-ray dips observed preferentially close to the phase 0. In our data, we have not seen any X-ray dips, which is consistent with the near uniformity of our measured values of N_H.

A. A. Z. has been supported in part by KBN grants 2P03C00511p0(1,4) and 2P03D00614 and a grant from the Foundation for Polish Science. We thank M. Gierliński for his assistance with the XSPEC software package, M. Guainazzi for his support with the LECS data analysis, J. Poutanen for comments on this paper, and G. Matt and S. N. Zhang for useful discussions. The *BeppoSAX* program is supported by the Italian Space Agency (ASI).

REFERENCES

Abramowicz, M. A., Chen, X., Kato, S., Lasota, J.-P., & Regev, O. 1995, ApJ, 438, L37
Anders, E., & Ebihara, M. 1982, Geochim. Cosmochim. Acta, 46, 2363
Arnaud, K. A. 1996, in ASP Conf. Series 101, Astronomical Data Analysis Software and Systems V, ed. G. H. Jacoby & J. Barnes (San Francisco: ASP), 17
Bałucińska-Church, M., Church, M. J., Charles, P. A., Nagase, F., LaSala, J., & Barnard R. 2000, MNRAS, 311, 861
Belloni, T., Méndez, M., van der Klis, M., Hasinger G., Lewin, W. H. G., & van Paradijs, J. 1996, ApJ, 472, L107
Beloborodov, A. M. 1999a, ApJ, 510, L123
———. 1999b, in ASP Conf. Series 161, High-Energy Processes in Accreting Black Holes, ed. J. Poutanen & R. Svensson (San Francisco: ASP), 295
Boella, G., Butler, R. C., Perola, G. C., Piro, L., Scarsi, L., & Bleeker, J. A. M. 1997a, A&AS, 122, 299
Boella, G., et al. 1997b, A&AS, 122, 327
Böttcher, M., & Liang, E. P. 1999, ApJ, 511, L37
Bregman, J., Butler, D., Kemper, E., Koski, A., Kraft, R. P., & Stone, R. P. S. 1973, ApJ, 185, L117
Brocksopp, C., Tarasov, A. E., Lyuty, V. M., & Roche, P. 1999, A&A, 343, 861
Coppi, P. S. 1992, MNRAS, 258, 657
———. 1999, in ASP Conf. Series 161, High-Energy Processes in Accreting Black Holes, ed. J. Poutanen & R. Svensson (San Francisco: ASP), 375
Cui, W. 1996, IAU Circ. 6404
Cui, W., Ebisawa, K., Dotani, T., & Kubota, A. 1998, ApJ, 493, L75
Cui, W., Zhang, S. N., Focke, W., & Swank, J. H. 1997, ApJ, 474, L57
Czerny, B., & Elvis, M. 1987, ApJ, 321, 305
Diplas, A., & Savage, B. D. 1994, ApJ, 427, 274
Dolan, J. F., Crannell, C. J., Dennis, B. R., Frost, K. J., & Orwig, L. E. 1977, Nature, 267, 813
Done, C., Mulchaey, J. S., Mushotzky, R. F., & Arnaud, K. A. 1992, ApJ, 395, 275
Done, C., Życki, P. T. 1999, MNRAS, 305, 457
Dotani, T., et al. 1997, ApJ, 485, L87
Ebisawa, K., Ueda, Y., Inoue, H., Tanaka, Y., & White, N. E. 1996, ApJ, 467, 419 (E96)
Esin, A. A., Narayan, R., Cui, W., Grove, J. E., & Zhang, S. N. 1998, ApJ, 505, 854
Fabian, A. C., Rees, M. J., Stella, L., & White, N. E. 1989, MNRAS, 238, 729
Frontera, F., Costa, E., Dal Fiume, D., Feroci, M., Nicastro, L., Orlandini, M., Palazzi, E., & Zavattini, G. 1997, A&AS, 122, 357
Ghisellini, G., & Haardt, F. 1994, ApJ, 429, L53
Gierliński, M., Zdziarski, A. A., Done, C., Johnson, W. N., Ebisawa, K., Ueda, Y., Haardt, F., & Phlips, B. F. 1997, MNRAS, 288, 958 (G97)
Gierliński, M., Zdziarski, A. A., Poutanen, J., Coppi, P. S., Ebisawa, K., & Johnson, W. N. 1999, MNRAS, 309, 496 (G99)
Gilfanov, M., Churazov, E., & Revnivtsev, M. 1999, A&A, 352, 182 (GCR99)
Haardt, F. 1993, ApJ, 413, 680
Hanawa, T. 1989, ApJ, 341, 948
Herrero, A., Kudritzki, R. P., Gabler, R., Vilchez, J. M., & Gabler, A. 1995, A&A, 297, 556
Janes, K., & Adler, D. 1982, ApJS, 49, 425
Laurent, P., & Titarchuk, L. 1999, ApJ, 511, 289
Liang, E. P., & Nolan, P. 1984, Space Sci. Rev., 38, 353
Maccarone, T. J., Coppi, P. S., & Poutanen, J. 2000, ApJ, 537, L107
Magdziarz, P., & Zdziarski, A. A. 1995, MNRAS, 273, 837
Malysheva, L. K. 1997, Astron. Lett., 23, 585 [in Russian: AZh Pis'ma, 23, 667]
Manzo, G., Giarrusso, S., Santangelo, A., Ciralli, F., Fazio, G., Piraino, S., & Segreto, A. 1997, A&AS, 122, 341
Margon, B., Bowyer, S., & Stone, R. P. S. 1973, ApJ, 185, L113
Massey, P., Johnson, K. E., & DeGioia-Eastwood, K. 1995, ApJ, 454, 151
McConnell, M. L., et al. 2000, in AIP Conf. Proc. 510, Fifth Compton Symposium, ed. M. L. McConnell & J. M. Ryan (New York: AIP), 114
Meyer, F., Liu, B. F., & Meyer-Hofmeister, E. 2000, A&A, 354, L67
Mitsuda, K., et al. 1984, PASJ, 36, 741
Narayan, R., & Yi, I. 1995, ApJ, 452, 710
Nayakshin, S. 2000, ApJ, 534, 718
Nayakshin, S., Kazanas, D., & Kallman, T. R. 2000, ApJ, 537, 833
Nolan, P. L., et al. 1981, Nature, 293, 275
Nowak, M. A. 1995, PASP, 107, 1207
Ogawara, Y., Mitsuda, K., Masai, K., Vallerga, J. V., Cominsky, L. R., Grunsfeld, J. M., Kruper, J. S., & Ricker, G. R. 1982, Nature, 295, 675
Palazzi, E., et al. 1999, Astrophys. Lett. Commun., 38, 253
Parmar, A. N., et al. 1997, A&AS, 122, 309
Phlips, B. F., et al. 1996, ApJ, 465, 907
Pottschmidt, K., Wilms, J., Nowak, M. A., Heindl, W. A., Smith, D. M., & Staubert, R. 2000, A&A, 357, L17
Poutanen, J. 1998, in Theory of Black Hole Accretion Discs, ed. M. A. Abramowicz, G. Björnsson, & J. E. Pringle (Cambridge: Cambridge Univ. Press), 100
Poutanen, J., & Coppi, P. S. 1998, Phys. Scr., T77, 57
Poutanen, J., Krolik, J. H., & Ryde, F. 1997, MNRAS, 292, L21
Poutanen, J., & Svensson, R. 1996, ApJ, 470, 249
Revnivtsev, M., Gilfanov, M., & Churazov, E. 1999, A&A, 347, L23
Różańska, A., & Czerny, B. 2000, A&A, 360, 1170
Shakura, N. I., & Sunyaev, R. A. 1973, A&A, 24, 337
Shapiro, S. L., & Lightman, A. P. 1976, ApJ, 204, 555
Sunyaev, R. A., & Trümper, J. 1979, Nature, 279, 506
Wen, L., Cui, W., & Bradt, H. V. 2000, ApJ, submitted; preprint (astro-ph/0011371)
Wen, L., Cui, W., Levine, A. M., & Bradt, H. V. 1999, ApJ, 525, 968
Wu, C.-C., Eaton, J. A., Holm, A. V., Milgrom, M., & Hammerschlag-Hensberge, G. 1982, PASP, 94, 149
Zdziarski, A. A. 2000, in IAU Symp. 195, Highly Energetic Physical Processes and Mechanisms for Emission from Astrophysical Plasmas, ed. P. C. H. Martens, S. Tsuruta, & M. A. Weber (San Francisco: ASP), 153
Zdziarski, A. A., Lubiński, P., & Smith, D. A. 1999, MNRAS, 303, L11
Zdziarski, A. A., Poutanen, J., Mikołajewska, J., Gierliński, M., Ebisawa, K., & Johnson, W. N. 1998, MNRAS, 301, 435
Zhang, S. N., et al. 1996, IAU Circ. 6405
———. 2000, Science, 287, 1239
Zhang, S. N., Cui, W., & Chen, W. 1997a, ApJ, 482, L155
Zhang, S. N., Cui, W., Harmon, B. A., Paciesas, W. S., Remillard, R. E., & van Paradijs, J. 1997b, ApJ, 477, L95
Życki, P. T., & Czerny, B. 1994, MNRAS, 266, 653